

Controls of dust emissions by vegetation and topographic depressions: An evaluation using dust storm frequency data

S. Engelstaedter, K. E. Kohfeld, I. Tegen, and S. P. Harrison

Max-Planck-Institute for Biogeochemistry, Jena, Germany

Received 17 October 2002; revised 15 January 2003; accepted 3 February 2003; published 21 March 2003.

[1] The degree to which dust emissions are controlled by vegetation cover and geomorphic setting (specifically closed topographic depressions) was investigated using dust storm frequency (DSF) data based on visibility measurements from >2400 meteorological stations worldwide. Comparisons with distributions of vegetation types suggest that DSF is highest in desert/bare ground (median: 60–80 d/yr) and shrubland (median: 20–30 d/yr) regions, and comparatively low in grassland regions (median: 2–4 d/yr). Average DSF is inversely correlated with leaf area index (an index of vegetation density) and net primary productivity. In non-forested regions, DSF increases as the fraction of closed topographic depressions increases, likely due to the accumulation of fine sediments in these areas. These findings support the importance of incorporating vegetation and geomorphic setting as explicit controls on emissions in global dust cycle models. **INDEX TERMS:** 0305 Atmospheric Composition and Structure: Aerosols and particles (0345, 4801); 0315 Atmospheric Composition and Structure: Biosphere/atmosphere interactions. **Citation:** Engelstaedter, S., K. E. Kohfeld, I. Tegen, and S. P. Harrison, Controls of dust emissions by vegetation and topographic depressions: An evaluation using dust storm frequency data, *Geophys. Res. Lett.*, 30(6), 1294, doi:10.1029/2002GL016471, 2003.

1. Introduction

[2] Surface winds and soil wetness are important controls on dust emission rates. However, global dust cycle models which determine emissions only on the basis of these factors generally require some empirical adjustments to reproduce observed dust concentrations and deposition rates. Regional studies suggest that land-surface characteristics, such as the nature of the vegetation cover and the geomorphic setting, are important controls on dust emission [e.g., Wyatt and Nickling, 1997; Gillette, 1999]. Recent global dust cycle models have attempted to incorporate the dependency of dust emissions on vegetation and/or the existence of geomorphically favorable emission sites such as topographic depressions [e.g., Ginoux *et al.*, 2001; Tegen *et al.*, 2002]. These simulations apparently reproduce more realistic patterns and amounts of dust in the atmosphere, and of dust deposition to the ocean, without requiring regional adjustments. However, the absence of a global data set of emission measurements has meant that there has been no direct attempt to determine the realism of the simulated regional emission rates using these new land-surface schemes. In this paper, we use dust storm frequency (DSF) data as a surrogate

for dust emissions to explicitly test the assumption that vegetation and topography are important controls of dust emission at a global scale.

2. Approach and Methods

2.1. Dust Storm Frequency (DSF) Data

[3] Meteorological observers define a dust storm as an occasion when visibility is reduced below a specified level because of the presence of dust in the near-surface layers of the atmosphere. The frequency of dust storms will thus be determined by the proximity of the recording station to a source and the strength of that source. Thus, DSF data can be used to provide a qualitative measure of the location and relative magnitude of dust sources.

[4] Our DSF data set is based on a climatological average of observations extracted from 2405 meteorological stations from the International Station Meteorological Climate Summary (ISMCS) version 4.0 [<http://navy.ncdc.noaa.gov/products/compactdisk/ismcs.html>]. The ISMCS is a pre-screened data set containing information processed from the original meteorological data codes. The data set contains a record of the average number of days (based on daily observations) on which dust storms occurred across the recording time interval, where a dust storm is defined as an event during which visibility was reduced to <1 km because of the presence of dust. The length of time for which meteorological records were available, and thus the number of years used for computation of the climatological average, varies from station to station. We excluded 31 stations with short (<8 years) records. Visibility at remote oceanic or ice sheet locations may be affected by shifts in dust-transport pathways but is clearly not influenced by local dust storms. We therefore excluded records from 106 remote island sites (e.g., Tenerife, Nassau) and 8 sites in Antarctica. Visibility records from large urban areas may be affected by factors other than proximity to dust sources, including dust generated by construction and pollution. We therefore excluded 11 records from stations in large urban areas (e.g., Manila, Mexico City). The climatology of the remaining 2249 stations is based on record lengths of 15–25 year average in >75% of the records. Most of the records cover the years between 1970 and 1990. Only in Australia and North America the time period of data coverage is longer, with median record lengths of 32 and 48 years, respectively.

[5] The DSF data show strong spatial patterns (Figure 1a). High DSFs (>50 days/year) are found in northern Africa (20W–30E, 10N–35N), the Middle East (30E–60E, 15N–35N) and the Iberian Peninsula (10W–5E, 5N–15N). Moderate to low DSFs (2–50 days/year) are found in Australia, eastern China, southern South America and the southwestern

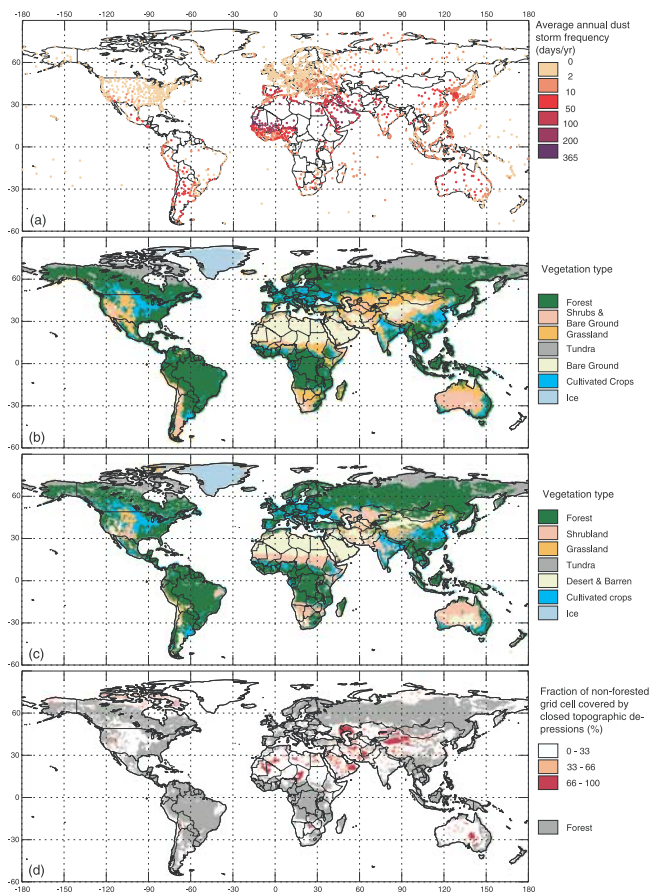


Figure 1. (a) Distribution and frequency of dust storms. (b) Vegetation types derived from NDVI based satellite data [DeFries and Townshend, 1994]. (c) Vegetation types simulated by BIOME4. (d) Distribution of closed topographic depressions as simulated by HYDRA in non-forested areas.

USA. The North American DSF values could be slightly inflated, because the records include the period of high dust storm activity in the 1950s [Goudie and Middleton, 1992]. Other areas have DSFs of <2 days/year.

2.2. Land-Surface Characteristics

[6] We investigated the relationship between DSF and vegetation using two independent determinations of global vegetation patterns: (1) a satellite-derived distribution of actual vegetation types [DeFries and Townshend, 1994], and (2) model-derived distribution of potential natural vegetation [Kaplan et al., 2003]. Given that the relationships between DSF and vegetation type established using both sources are consistent, the use of a model enables us to examine the impact of variation in vegetation cover, density and productivity within specific biomes on DSF.

[7] The DeFries and Townshend [1994] data set is a satellite-derived global vegetation map, based on interannual variations in the Normalized Difference Vegetation Index (NDVI) at a 1° by 1° resolution. Eleven vegetation types are distinguished. For the purpose of our analyses, the six forest vegetation types (*broadleaf evergreen forest*, *coniferous evergreen forest & woodland*, *high latitude deciduous forest & woodland*, *mixed forest*, *wooded grassland*, and *broadleaf deciduous forest & woodland*) were combined into a single

category (*forest*). Areas identified as *cultivated crops* were excluded, in order to focus on the impacts of natural vegetation on dust emission. The DeFries and Townshend [1994] data set does not explicitly distinguish ice sheets from areas of sparse tundra vegetation. We therefore applied an ice mask derived from the Food and Agricultural Organization (FAO) soils data set [after Kaplan et al., 2003] to exclude ice-covered areas from our analyses. Finally, the DeFries and Townshend [1994] data set was regridded to a 0.5° by 0.5° resolution (Figure 1b) to facilitate comparisons with the other data sets.

[8] BIOME4 is an equilibrium vegetation model that successfully simulates potential natural vegetation as a function of temperature, precipitation, net radiation, and soil type at a 0.5° by 0.5° resolution [Kaplan et al., 2003]. The model distinguishes 27 vegetation types. For comparison with the DSF data, these vegetation types were reclassified by grouping together biomes with similar physical characteristics. Thus *desert* and *barren* biomes were combined; *tropical grassland*, *temperate grassland*, and *graminoid and forb tundra* were grouped as *grassland*; *tundra biomes tundra low- and high-shrub tundra*, *erect dwarf-shrub tundra*, *prostrate dwarf-shrub tundra*, and *cushion-forb, lichen, and moss tundra*, were grouped as *tundra*; and *tropical xerophytic shrubland*, and *temperate xerophytic shrubland* were grouped as *shrubland*. All the forest biome types were classified as *forest*. Simulated net primary productivity (NPP, $\text{gC}/\text{m}^2/\text{yr}$), leaf area index (LAI, m^2/m^2), and the fraction of photosynthetically absorbed radiation (FPAR, %) were used to characterize variation in vegetation cover and density within each biome type. Ice-covered and cultivated areas were excluded from the analysis (Figure 1c) by applying the ice and cultivated crop masks used with the DeFries and Townshend [1994] data set.

[9] Not all sparsely-vegetated land surfaces emit dust [Gillette, 1999]. Observations suggest that topographic depressions containing easily deflatable, fine sediments act as preferential sources of dust emissions [Prospero et al., 2002]. To test whether these observations can be generalized to the global scale, we compare our DSF data with a model-derived global map of closed topographic lows [Figure 1d, after Tegen et al., 2002]. This map was derived using HYDRA (HYDrological Routing Algorithm: Coe [1998]), a water routing model that combines climatological information with a high-resolution ($5'$ by $5'$) land-surface topography to predict the accumulation of water in lakes and wetlands. The maximum extent of closed depressions was determined by running the model with unlimited precipitation. The fraction of a grid cell covered by the closed depressions was estimated after excluding all regions currently covered by lakes and by forests (as estimated by BIOME4), to exclude the effect that dust storms are suppressed when the vegetation cover is high. It is possible that the model over-predicts the occurrence of enclosed depressions because of inaccuracies in the underlying topographic data. Nevertheless, even areas that are not fully enclosed may still behave as sediment catchments and therefore act as preferential sources.

[10] Analysis of the relationships between land-surface variables and DSF was made at the location of the ISMCS meteorological stations. Although we have regridded the DeFries and Townshend [1994] and HYDRA data to the common 0.5° by 0.5° grid, we did not fill missing grid cells

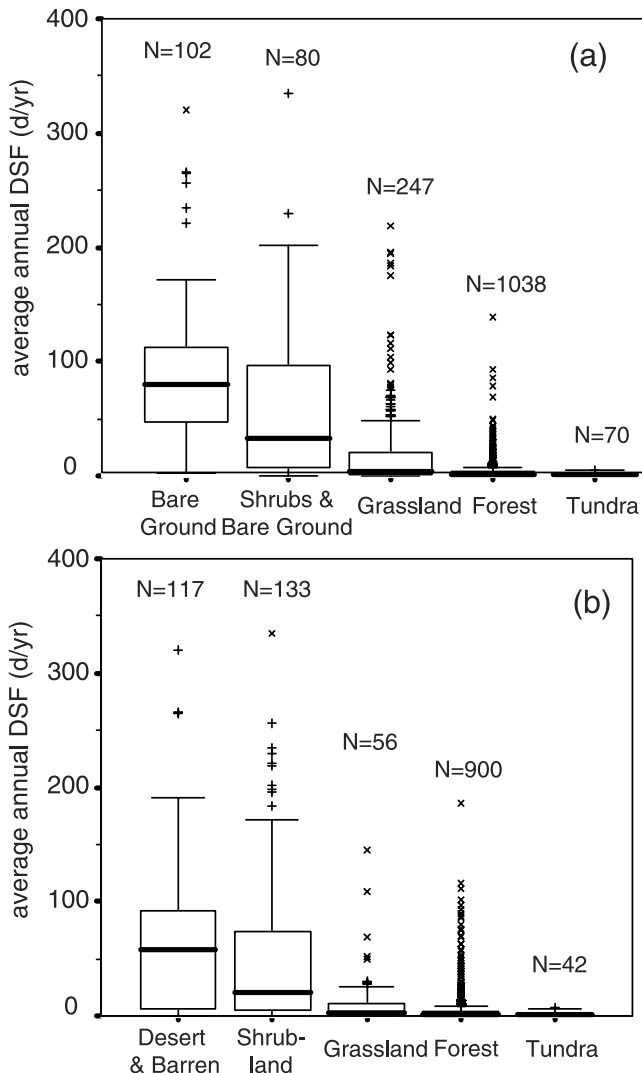


Figure 2. Correlation between average annual DSF and different vegetation types derived from (a) the *DeFries and Townshend* [1994] data set, and (b) the BIOME4 simulation. The horizontal line through the box represents the median, the lower edge of the box the 25%-percentile and the upper edge the 75%-percentile. The horizontal lines below and above the box represent the minimum value and maximum value not including outliers and extreme values (+ = Outliers; x = Extreme Values) [Pospeschill, 2001].

by interpolation. As a result, data was available from the *DeFries and Townshend* [1994] data set at only 1537 ISMCS stations, and from BIOME4 at only 1248 ISMCS stations. Data on the extent of closed depressions were extracted from the HYDRA model for non-forest areas, leaving only 348 ISMCS stations.

3. Results

[11] The highest DSFs (Figure 2a) are found in areas mapped by *DeFries and Townshend* [1994] as *bare ground* (median DSF $m = 79.4$ d/yr). Moderate DSFs occur in regions with more vegetation, i.e. *shrubs & bare ground* ($m = 32.5$ d/yr), and lowest DSFs occur in *grasslands* ($m = 3.7$ d/yr), *forests* ($m = 1.5$ d/yr), and *tundra* ($m = 1.1$ d/yr). A

similar pattern emerges with the simulated BIOME4 vegetation types (Figure 2b). Highest DSFs are found in *desert & barren* regions ($m = 58.1$ d/yr); moderate DSFs occur in *shrubland* vegetation ($m = 20.8$ d/yr); lowest DSFs are associated with *grassland* ($m = 2.2$ d/yr), *tundra* ($m = 1.6$ d/yr), and *forest* ($m = 1.5$ d/yr). The differences in median DSF between the individual vegetation types are all statistically significant at the 0.01 level, except for the difference in median DSF of the *forest* and *tundra* vegetation types of the *DeFries and Townshend* [1994] dataset, and the *grassland* and *tundra* vegetation type of the BIOME4 dataset (both significant at the 0.05 level), and the difference in median DSF between *forest* and *tundra* vegetation in the BIOME4 data set, which is not statistically significant.

[12] The relationship between vegetation type and DSF reflects the fact that different vegetation types are characterized by differences in density and structure. Forested regions for example have relatively high biomass and vegetation cover. The density of the vegetation protects the surface from deflation, while the presence of trees results in a high surface roughness that reduces surface wind energy and therefore also dust emissions. In contrast, shrublands tend to have less dense vegetation and more bare soil. This results in a larger unprotected area with a lower surface roughness and therefore increased potential for dust emissions. Indeed, the relationships between DSFs and NPP, FPAR, and LAI (Figures 3a–3c) show that variations in the density of vegetation cover within specific biomes have a significant

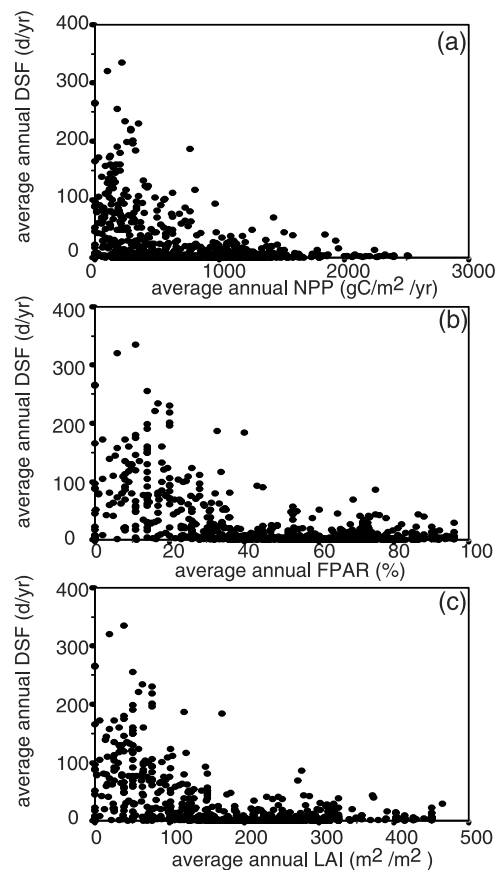


Figure 3. Correlation between average annual DSF and simulated (a) NPP, (b) FPAR, and (c) LAI derived from the BIOME4 simulation.

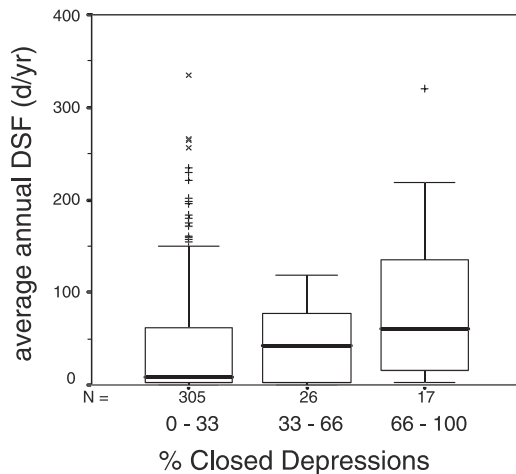


Figure 4. Correlation between average annual DSF and grouped percentage of grid cell area covered by closed topographic depressions simulated by HYDRA.

impact on dust emission. DSF is inversely related to all three measures of vegetation density (Spearman coefficients of -0.2 , -0.33 , and -0.3 respectively; significant at the 0.01 level). DSF variability is highest at low values of NPP, FPAR, and LAI (Figures 3a–3c), reflecting the fact that maximum levels of dust deflation can only occur under low vegetation density when permitted by other surface conditions (e.g. high winds and surface dryness).

[13] In non-forested areas, DSF increases as the fractional area of closed depressions increases (Figure 4, Spearman coefficient = 0.13; significant at the 0.05 level). DSFs are lowest ($m = 8.4$ d/yr) when <33% of a grid cell is covered by topographic depressions, and highest ($m = 61.0$ d/yr) in regions with >66% coverage. Intermediate values ($m = 42.4$ d/yr) are found for areas with 33–66% coverage. This suggests that topographic depressions and closed basins, which represent regions likely to accumulate easily deflatable sediments, are preferential sources of dust.

4. Discussion and Conclusions

[14] This study uses DSF data derived from visibility records from meteorological stations to evaluate the controls on dust emissions. There are large differences in DSF between different vegetation types; it should be possible to parameterize these relationships to first order within global dust cycle models by prescribing vegetation-specific emission rates. However, as the strong correlation between DSF and NPP, LAI, and FPAR shows, there is significant variability in emissions within vegetation types. Thus, it would be better to simulate these vegetation characteristics explicitly within dust cycle models. Our analyses support the hypothesis that DSF increases as the extent of closed depressions in non-forested areas increases. Thus, the incorporation of these preferential sources should also lead to improved simulation of dust emissions.

[15] The DSF data set used here reproduces the regional DSF patterns shown in previous regional studies using similar approaches with meteorological visibility data [e.g. Changery, 1983; Goudie, 1983; Middleton, 1984, 1986; Wheaton and Chakravarti, 1990]. The global DSF data set has the advantage of internal consistency and there are

none of the artificial discontinuities along political boundaries, which show up when the regional data sets are combined. The robustness of the regional patterns compared more detailed regional compilations demonstrate the reliability of the ISMCS compilation; the internal consistency permits derivation of quantitative global-scale relationships.

[16] Processes other than local dust storms can affect visibility, e.g. anthropogenic dust, or changes in long-distance dust-transport pathways. We have screened out stations obviously affected by these processes, but it is not possible to do this systematically and some stations in the data set could still be affected. The ISMCS data set distinguishes reduced visibility due to smoke from reduced visibility due to dust. However, it is still possible that the estimated DSFs may be inflated by biomass burning events. Anthropogenic dust, biomass burning and changes in long-distance transport pathways are likely to decrease visibility over regions with high vegetation cover. Thus, the fact that we see a significant relationship between land-surface characteristics and DSF suggests that the potential problems are relatively unimportant.

[17] **Acknowledgments.** We thank G. McTainsh for helpful comments, R. Gaupp for productive discussions, M. Horn for statistical advice, and G. Boenisch for help with data handling. The ISMCS data are available from the National Oceanic & Atmospheric Administration (NOAA, <http://www4.ncdc.noaa.gov/cgi-win/wwwcgi.dll?wwAW-MP-CD>). This work was supported by the Max Planck Institute for Biogeochemistry, Jena, Germany.

References

- Changery, M. J., A dust climatology of the western United States, Natl. Data Cent. for Clim., Asheville, N. C., 1983.
- Coe, M. T., A linked global model of terrestrial hydrologic processes: Simulation of modern rivers, lakes, and wetlands, *J. Geophys. Res.*, *103*, 8885–8899, 1998.
- DeFries, R. S., and J. R. G. Townshend, NDVI-derived land cover classification at a global scale, *Int. J. Remote Sens.*, *15*, 3567–3586, 1994.
- Gillette, D. A., A qualitative geophysical explanation for “hot spot” dust emitting source regions, *Contrib. Atmos. Phys.*, *72*, 67–77, 1999.
- Ginoux, P., M. Chin, I. Tegen, J. M. Prospero, B. Holben, O. Dubovik, and S.-J. Lin, Sources and distributions of dust aerosols simulated with the GOCART model, *J. Geophys. Res.*, *106*, 20,225–20,273, 2001.
- Goudie, A. S., Dust storms in space and time, *Prog. Phys. Geogr.*, *7*, 503–530, 1983.
- Goudie, A. S., and N. J. Middleton, The changing frequency of dust storms through time, *Clim. Change*, *20*, 197–225, 1992.
- Kaplan, J. O., et al., Climate change and arctic ecosystems: 2. Modeling, paleodata-modeling comparisons, and future projections, *J. Geophys. Res.*, doi:10.1029/2002JD002559, in press, 2003.
- Middleton, N. J., Dust storms in Australia: Frequency, distribution and seasonality, *Search*, *15*, 46–47, 1984.
- Middleton, N. J., Dust storms in the Middle East, *J. Arid Environ.*, *10*, 83–96, 1986.
- Pospeschill, X., SPSS für Fortgeschrittene, Univ. of Hannover, Hannover, Germany, 2001.
- Prospero, J. M., P. Ginoux, O. Torres, S. E. Nicholson, and T. E. Gill, Environmental characterization of global sources of atmospheric soil dust identified with the NIMBUS 7 Total Ozone Mapping Spectrometer (TOMS) absorbing aerosol product, *Rev. Geophys.*, *40*(1), 1002, doi:10.1029/2000RG000095, 2002.
- Tegen, I., S. P. Harrison, K. E. Kohfeld, I. C. Prentice, M. Coe, and M. Heimann, Impact of vegetation and preferential source areas on global dust aerosol: Results from a model study, *J. Geophys. Res.*, *107*(D21), 4576, doi:10.1029/2001JD000963, 2002.
- Wheaton, E. E., and A. K. Chakravarti, Dust storms in the Canadian prairies, *Int. J. Climatol.*, *10*, 829–837, 1990.
- Wyatt, V. E., and W. G. Nickling, Drag and shear stress partitioning in sparse desert creosote communities, *Can. J. Earth Sci.*, *34*, 1486–1498, 1997.